ACE2 and a Traditional Chinese Medicine Formula NRICM101 Could Alleviate the Inflammation and Pathogenic Process of Acute Lung Injury

Cheng-Han Lin , Yi-Ju Chen , Meng-Wei Lin * , Ho-Ju Chang , Xin-Rui Yang , Chih-Sheng Lin *

Posted Date: 17 July 2023

doi: 10.20944/preprints202307.1065.v1

Keywords: Acute lung injury (ALI); Angiotensin-converting enzyme type II (ACE2); Animal model; traditional Chinese medicine

Article

ACE2 and a Traditional Chinese Medicine Formula NRICM101 Could Alleviate the Inflammation and Pathogenic Process of Acute Lung Injury

Cheng-Han Lin [1], Yi-Ju Chen [1], Meng-Wei Lin [1], Ho-Ju Chang [1], Xin-Rui Yang [1] and Chih-Sheng Lin [1,2,3,*]

[1] Department of Biological Science and Technology, National Yang Ming Chiao Tung University, Hsinchu 30068, Taiwan; a0975273923@gmail.com (C.-H.L.); tam13053@gmail.com (Y.-J.C.); lmw1018@nycu.edu.tw (M.-W.L.); imhrchang@gmail.com (H.-J.C); yllas0315@gmail.com (X.-R.Y.); lincs@nycu.edu.tw (C.-S.L.)

[2] Department of Biological Science and Technology, National Chiao Tung University, Hsinchu 30068, Taiwan

[3] Center for Intelligent Drug Systems and Smart Bio-devices (IDS²B), National Yang Ming Chiao Tung University, Hsinchu 30068, Taiwan

* Correspondence: lincs@nycu.edu.tw (C.-S.L.); Tel.: +886-3-513-1338

Abstract: COVID-19 is a highly infectious respiratory illness caused by SARS-CoV-2, and acute lung injury (ALI) is the major cause of COVID-19. The challenge in studying SARS-CoV-2 pathogenicity is the limited availability of animal models. Therefore, it is necessary to establish animal models that can reproduce multiple characteristics of ALI to study therapeutic applications. The present study established a mouse model that has features of ALI that are similar to COVID-19 syndrome to investigate the role of ACE2 and the administration of the Chinese herbal prescription NRICM101 in ALI. Mice with genetic modifications, including overexpression of human ACE2 (K18-hACE2 TG) and absence of ACE2 (mACE2 KO), were intratracheally instillated with hydrochloric acid. The acid intratracheal instillation induced severe immune cell infiltration, cytokine storms, and pulmonary disease in mice. Compared with K18-hACE2 TG mice, mACE2 KO mice exhibited dramatically increased levels of multiple inflammatory cytokines (IL-6, TNF-α, and TGF-β1) in bronchoalveolar lavage fluid, histological evidence of lung injury, and dysregulation of MAPK and MMP activation. In mACE2 KO mice, NRICM101 could ameliorate the disease progression of acid-induced ALI. In conclusion, the established mouse model provided an effective platform for researchers to investigate pathological mechanisms and develop therapeutic strategies for ALI, including COVID-19-related ALI.

Keywords: Acute lung injury (ALI); Angiotensin-converting enzyme type II (ACE2); Animal model; traditional Chinese medicine

1. Introduction

The renin-angiotensin system (RAS) plays a central role in regulating blood pressure homeostasis and electrolyte balance [1,2]. Abnormal activation of the RAS is associated with the pathogenesis of many diseases [2]. The protease renin cleaves angiotensinogen to generate angiotensin I (Ang I). Angiotensin converting enzyme (ACE) is a critical protease that regulates the RAS by cleaving Ang I to generate angiotensin II (Ang II), which is a key regulator of the RAS and exerts biological effects through the specific receptor Ang II receptor type 1 (AT1R) [1]. Thus, ACE is a key enzyme in ACE-Ang II/AT1R signaling in the regulation of RAS [3,4]. In 2000, a homolog of ACE was cloned and termed angiotensin converting enzyme II (ACE2) [5,6]. While ACE cleaves Ang I into Ang II, ACE2 removes a single residue from Ang II to generate angiotensin (1-7) (Ang-(1-7)). Studies indicated a counter regulatory role for Ang-(1-7) via its specific receptor Mas by opposing many AT1R-mediated effects [7–9]. Thus, ACE2-Ang-(1-7)/Mas signaling has emerged as a potent

negative regulator of ACE-Ang II/AT1R in the RAS, playing an opposing role to ACE in various organ systems, including the heart, kidneys and lungs [2,10,11]. Based on its physiological functions, ACE2 is considered a protector of the RAS [8].

In December 2019, Severe Acute Respiratory Syndrome Coronavirus 2 (SARS-CoV-2) and coronavirus disease (COVID-19) outbreak occurred in Wuhan, China [12]. As of March 2023, COVID-19 has infected more than 676 million people and caused the death of over 6 million people worldwide [13]. The COVID-19 pandemic has posed severe threats to populations, social structures, and economic growth [14]. Nevertheless, over the past three years, it is still prudent to accelerate investigations of new therapeutic advances that can effectively treat COVID-19. SARS-CoV-2 enters human cells by the binding of its spike protein to ACE2 on the cell membrane [15]. In addition to the role of ACE2 in viral entry, the interaction between the viral spike protein and ACE2 leads to the development of severe symptoms of COVID-19, such as inflammation and acute lung injury (ALI) [15]. ACE2 depletion by SARS-CoV-2 spike protein binding disrupts the balance between ACE and ACE2 (i.e., ACE/ACE2) and increases the level of Ang II [16]. This could contribute to the development of ALI patients, as well as other complications of COVID-19 [17,18].

ACE2 is a SARS-CoV-2 entry receptor, which suggests that the increase in ACE2 expression may lead to an increase in cell infection [19]. ACE2 also plays a key role in balancing the tissue RAS against antioxidation, anti-inflammatory and antifibrotic responses through ACE2-Ang-(1-7)/Mas signaling [20,21]. This raised the initial dilemma of whether we should increase ACE2 levels in the lungs to inhibit the injury process or reduce tissue ACE2 levels to decrease SARS-CoV-2 entry and replication. This has been termed the double-edged sword of ACE2 [22–24]. One of the challenges in studying the double-edged sword of ACE2 related to SARS-CoV-2 pathogenicity is the limited availability of animal models. Another challenge is the highly infective nature of SARS-CoV-2, and handling and experimentation using this virus must be conducted in a biosafety level 3 (BSL-3) facility [25]. It is fortunate that human ACE2 transgenic (hACE2 TG) and murine ACE2 knockout (mACE2 KO) mice have been generated. Both types of mice are reasonable animal and translational models for studying SARS-CoV-2 infection and COVID-19-related ALI pathogenesis [26,27]. Therefore, hACE2 TG and mACE2 KO mice were used in the present study to examine ACE2 and ALI.

The most common and severe complication of COVID-19 is ALI, which can lead to respiratory failure and death [28]. ALI is characterized by the induction of inflammatory cytokines, is associated with COVID-19 severity and is a crucial cause of death from COVID-19 [29]. Traditional Chinese medicine (TCM) has long been used to modulate immunity and suppress inflammation, particularly in lung diseases [30,31]. Therefore, TCM and Western medicine can be used in combination to treat lung damage caused by SARS-CoV-2, and TCM effectively provides continuous prevention and treatment of COVID-19 [32,33]. In Taiwan, Chingguan Yihau (NRICM101), which is an effective TCM, exerts both antiviral and anti-inflammatory effects against COVID-19 [34]. Tsai et al. [34] pointed out that pharmacological assays demonstrated the effects of NRICM101 on inhibiting the SARS-CoV-2 spike protein/ACE2 interaction. However, no further studies have explored the therapeutic mechanism and effects of TCM on ACE2 regulation.

In this study, ALI was induced in hACE2 TG and mACE2 KO mice by intratracheal instillation of hydrochloric acid (HCl) to explore the relationship between ACE2 and ALI pathogenesis. Intratracheal instillation of HCl could be used to induce ALI in a mouse model [35,36]. Our results showed that the pathological features of acid-induced ALI were similar to those of COVID-19-related lung damage. Therefore, the effects of NRICM101 administration on acid-induced ALI were evaluated in animal models in this study.

2. Materials and Methods

2.1. Cell line and cell culture

The human lung adenocarcinoma cell line A549 was obtained from the American Type Culture Collection (Manassas, VA, USA). A549 cells were cultured in Dulbecco's modified Eagle's medium (DMEM) with 10% fetal bovine serum (FBS) and maintained in a humidified atmosphere of 5% CO_2

Preprints (www.preprints.org) | NOT PEER-REVIEWED | Posted: 17 July 2023 doi:10.20944/preprints202307.1065.v1

at 37°C. The cells were washed with Dulbecco's phosphate buffered saline (DPBS) and detached from the culture surface using 0.25% trypsin-EDTA solution for subculture and seeding.

2.2. Acid and NRICM101 treatment of cells

A549 cells were cultured in complete medium for 24 h in the Control group. The cells were treated with 0.5 mg/mL NRICM101 (Sun Ten Pharmaceutical Co., Taipei, TW) for 24 h in the TCM only group. The cells were treated with 0.1 N HCl for 30 min and then placed in culture medium for 24 h in the Acid group. The cells were treated with 0.1 N HCl (pH = 4) for 30 min and then placed in 0.5 mg/mL NRICM101 for 24 h in the NRICM101 group.

2.3. Determination of cell viability

The 3-(4,5-dimethylthiazol-2-yl)-2,5-diphenyl tetrazolium bromide (MTT) assay is a standard method for determining cell viability. A549 cells were seeded in 96-well plates (4×10^4 cells/well) and incubated at 37 °C and humidified 5% CO_2 for 24 h. Following attachment, the cells were treated with different conditions. Subsequently, the medium was removed, and the cells were incubated with 5 mg/mL MTT solution for 4 h. The supernatant in the wells was aspirated, and dimethyl sulfoxide (DMSO) was added to dissolve the purple formazan crystals. Finally, the absorbance of the produced formazan solution was measured at 570 nm (BioTek Instruments, Winooski, VT, USA). The results are expressed as the cell viability (%) relative to the Control group.

2.4. Determination of ROS production

DCFH-DA (Sigma Life Science, St. Louis, MO, USA) is a fluorogenic dye. DCFH-DA penetrated the cell membrane and was hydrolyzed by esterase to form a nonfluorescent compound. DCFH-DA was added to A549 cells and placed in an incubator for 30 min. Then, the cells were washed twice with DPBS, and the cells were resuspended in 0.25% trypsin-EDTA. ROS production in A549 cells was analyzed by a fluorescence spectrophotometer (F-2700; Hitachi High Technologies, Pleasanton, CA, USA) at excitation and emission wavelengths of 488 and 525 nm, respectively.

2.5. Animal model

Three genotypes of mice were used in this study: WT, K18-hACE2 TG [strain: B6. Cg-Tg (K18-ACE2)2Prlmn/J], and mACE2 KO (B6;129S5-Ace2tm1Lex/Mmcd). WT and K18-hACE2 TG mice were purchased from the Jackson Laboratory (Jax, Bar Harbor, ME, USA). The first generation of K18-hACE2 TG mice was bred at Bio-LASCO (Taipei, Taiwan) and identified by DNA genotyping. mACE2 KO mice were obtained from Mutant Mouse Regional Resource Centers (MMRRC; Jax). Twelve-week-old WT, K18-hACE2 TG and mACE2 KO male mice were divided into the Control, Acid and Acid+TCM groups (n = 5 for each group; a total of 45 mice used) in this study (Table 1). All animal experiments conformed to the "Guide for the Care and Use of Laboratory Animals published by National Institutes of Health" (NIH Publication No. 85-23, revised 1996) and were approved by the Animal Welfare Committee of National Chiao Tung University (NCTU-IACUC-110002).

Table 1. Groups of *in vivo* experimental mice.

Mice	Group	n	PBS	Acid	NRICM101
WT	Control	5	+	–	–
	Acid	5	–	+	–
	Acid+TCM	5	–	+	+
K18-hACE2 TG	Control	5	+	–	–
	Acid	5	–	+	–
	Acid+TCM	5	–	+	+
mACE2 KO	Control	5	+	–	–
	Acid	5	–	+	–

Preprints (www.preprints.org) | NOT PEER-REVIEWED | Posted: 17 July 2023 doi:10.20944/preprints202307.1065.v1

Acid+TCM	5	–	+	+

2.6. Acid and NRICM101 treatment of animals

In the Acid group, the mice were treated with 0.1 N HCl via intratracheal instillation once every three days for a total of two times (2 μL/g of body weight). In the Acid+TCM group, the mice were treated twice with acid intratracheal instillation and then treated with NRICM101 by oral gavage for 4 days (3 g/kg of body weight/day). The Control group was treated with PBS (Gibco-Invitrogen, Paisley, UK) via intratracheal instillation. The experiment was divided into 3 groups (n = 5), all mice were sacrificed 4 days after intratracheal instillation, and physiopathological examinations of the lungs were performed. TST and FST were used to evaluate animal activity. Body weight, TST and FST were measured daily before the animals were sacrificed.

2.7. EBD extravasation

Lung vascular permeability was evaluated by measuring EBD leakage. The mice were treated with EBD (Santa Cruz, Dallas, TX, USA) by intratracheal instillation 1 h before being euthanized. The lungs were isolated, weighed, and incubated with formamide (500 μL) at 55 °C for 48 h to extract the dye. The formamide and EBD mixture was centrifuged to pellet any remaining tissue fragments. The optical density was spectrophotometrically determined at 620 nm (Thermo Scientific, Waltham, MA, USA).

2.8. Lung histopathology

Lung tissues were isolated from WT, K18-hACE2, and mACE2 KO mice, fixed in 10% formaldehyde overnight, embedded in paraffin, and cut into 6 μm-thick sections on acid-pretreated slides for H&E and Masson's trichrome staining. The stained pathological sections were photographed by a digital camera mounted on a microscope. A computerized microscope equipped with a high-resolution video camera (BX 51; Olympus, Tokyo, Japan) was used for morphometric analysis.

2.9. Enzyme-linked immunosorbent assay (ELISA)

Lung IL-6, TNF-α, and TGF-β1 levels were detected by sandwich ELISA kits (Abcam, Cambridge, MA, USA). Homogenates of mouse lung tissue were incubated in 96-well ELISA plates with primary antibodies. After the addition of biotinylated capture antibodies, the plates were washed and reacted with HRP-conjugated streptavidin. Tetramethylbenzidine (TMB) was used to detect IL-6, TNF-α or TGF-β1, and the results were measured at 450 nm using a microplate reader (Thermo Scientific).

2.10. Western blotting

Lung homogenates with an equivalent protein content of 25 μg were separated by 12% sodium dodecyl sulfate–polyacrylamide gel electrophoresis (SDS–PAGE) and then transferred to polyvinylidene fluoride membranes (Immo-bilon-PTM; Millipore, Bedford, MA, USA). Primary antibodies against ACE were obtained from Genetex (Irvine, CA, USA); p-STAT3, p-ERK1/2 and β-actin were purchased from Cell Signaling Technology (Beverly, MA, USA).

Immunoreactivity was detected by enhanced chemiluminescence (Immobilon Western Chemiluminescent HRP Substrate; Millipore, Billerica, MA, USA). PAGE membranes were exposed in Lumi-Film Chemiluminescent Detection Film (Roche, Indianapolis, IN, USA). Band density was measured with Scion Image software (Scion, Frederick, MD, USA). The levels of ACE, p-ERK1/2 and p-STAT3 were normalized to β-actin.

 doi:10.20944/preprints202307.1065.v1

2.11. Gelatin zymography

Lung homogenates were mixed with zymography sample buffer (0.375 M Tris-HCl, pH 6.8, 20% (v/v) glycerol, 12% (w/v) SDS, and 0.015% bromophenol blue), incubated for 10 min at 37°C, and loaded into 10% acrylamide gels containing 0.1% (w/v) gelatin (Sigma–Aldrich). After electrophoresis, the gel was washed twice with zymography renaturing buffer (2.5% Triton X-100) for 30 min and incubated in developing buffer (50 mM Tris-HCl, pH 7.4, 200 mM NaCl, 5 mM $CaCl_2$, and 0.02% Brij35) for 20 h at 37°C. Then, the gels were stained with Coomassie blue for 30 min and further destained with destaining buffer (50% methanol, 10% acetic acid, and 40% ddH_2O). The activity of MMP-2 and MMP-9 in lung tissue was determined on the basis of clear or unstained areas, which are indicative of enzyme activity on the gelatin substrate. The unstained areas were quantified by using Scion Image software (Scion).

2.12. Statistical analysis

All values are expressed as the mean ± standard deviation (SD). Student's t test was performed for comparisons between two groups. One-way analysis of variance (ANOVA) was performed to evaluate differences among multiple groups.

3. Results

3.1. NRICM101 promoted viability and reduced oxidative stress in acid-treated A549 cells

To investigate the potential of the TCM NRICM101 to alleviate cytotoxicity and oxidative stress resulting from acid treatment in the lung cell line A549, we subjected the cells to acid (0.1 N HCl; pH = 4) for 30 min, followed by the administration of NRICM101 for 24 h. Subsequently, cell viability in the TCM only (i.e., only treatment by NRICM101), Acid and Acid+TCM groups were 97, 68 and 87%, respectively, compared to the Control group (**Figure 1**a). To assess the level of intracellular reactive oxygen species (ROS) following acid and NRICM101 treatment, 2,7-dichlorofluorescin (DCF)-derived fluorescence was used to analyze cellular ROS levels. The DCF-derived fluorescence in the TCM only, Acid and Acid+TCM groups was 1.5-, 6.0- and 4.2-fold higher, respectively, than that in the Control group (**Figure 1**b,c).

Preprints (www.preprints.org) | NOT PEER-REVIEWED | Posted: 17 July 2023 doi:10.20944/preprints202307.1065.v1

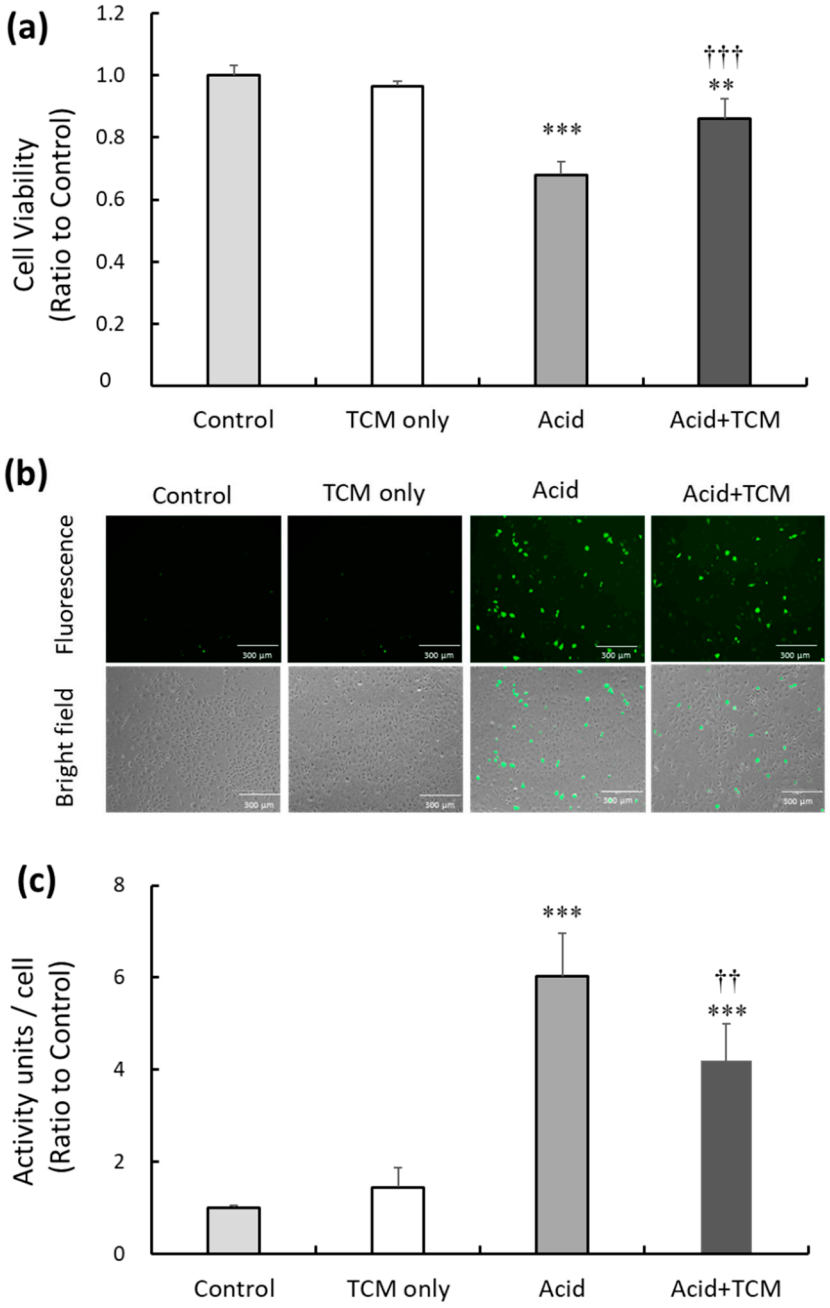

Figure 1. Effect of TCM and NRICM101 treatment on cell viability and ROS production in A549 cells exposed to acidic medium. (a) Cell viability in the Control, TCM only, Acid and Acid+TCM groups was detected by MTT assays. Cell viability in the nonacid and non-NRICM101 treatment groups was calculated as 100% and defined as the control value. The cells were treated with medium containing HCl (pH = 4) for 30 min in Acid group, and then treated with 0.5 mg/mL NRICM101 for 24 h in Acid+TCM group. (b) The level of ROS in A549 cells was measured by DCF fluorescence, and photographs of 2,7-dichlorofluorescin diacetate (DCFH-DA)-stained A549 cells are shown. (c) Histogram values reflect the mean ± SD (n = 5 for each treatment), and the values in the plots are the relative DCFH-DA-derived activity units/cell fluorescence relative to the Control group, which was 1. $^{**}p < 0.01$ and $^{***}p < 0.001$ *vs*. Control group; †† $p < 0.01$ and †††$p < 0.001$ *vs*. Acid group. Control group: A549 cells cultured in complete medium for 24 h. TCM only group: The cells were treated with 0.5 mg/mL NRICM101 for 24 h. Acid group: The cells were treated with 0.1 N HCl (pH = 4) for 30 min. Acid+TCM group: The cells were treated with 0.1 N HCl for 30 min and then placed in medium containing 0.5 mg/mL NRICM101 for 24 h.

 doi:10.20944/preprints202307.1065.v1

3.2. ACE2 and NRICM101 enhanced vitality in mice with acid-induced ALI

C57BL/6 mice (wild type, WT), K18-hACE2 transgenic mice (K18-hACE2 TG), and mACE2 knockout mice (mACE2 KO) were treated with PBS by intratracheal instillation twice in the Control group. The mice were treated with acid intratracheal instillation twice in the Acid group, and treated with acid intratracheal instillation twice and then administered NRICM101 for 4 days in the Acid+TCM group (**Table 1**). The health, body weight and vitality of the animals were monitored daily until sacrifice. Body weight was markedly decreased throughout the entire period of acid intratracheal instillation and slightly recovered after the cessation of acid instillation. Notably, mACE2 KO mice that were intratracheally instillated with acid exhibited a rapid and sustained declines in body weight compared with the other mice. However, the administration of NRICM101 did not significantly affect the body weight of the mice (**Figure 2**a).

The effects of ACE2 and NRICM101 on acid-induced ALI mice were examined by the tail suspension test (TST) and forced swimming test (FST), and the results are shown in **Figure 2**b and **Figure 2**c. In the Acid group, the TST results of WT, K18-hACE2 TG and mACE2 KO mice were significantly reduced by approximately 76, 86 and 67%, respectively, and the FST results of WT, K18-hACE2 TG and mACE2 KO mice were significantly reduced by approximately 75, 90 and 62%, respectively, compared with those in the Control group. In the Acid+TCM group, the TST and FST results of WT, K18-hACE2 TG and mACE2 KO mice were increased by approximately 86, 89 and 83% and 89, 97 and 86% compared with those in the Control group, respectively. The acid-induced ALI mice that were administered NRICM101 exhibited effectively increased vitality.

WT, K18-hACE2 TG and mACE2 KO mice were treated twice with PBS intratracheal instillation (Control group). The mice were treated twice with acid intratracheal instillation (Acid group). The mice were treated twice with acid intratracheal instillation twice and then administered NRICM101 for 4 days (Acid+TCM group). For acid intratracheal instillation, 0.1 N HCl was intratracheally instillated once every three days, twice in total (2 μL/g of body weight). For NRICM101 administration, NRICM101 was administered consecutively for 4 days (3 g/kg of body weight/day).

Preprints (www.preprints.org) | NOT PEER-REVIEWED | Posted: 17 July 2023 doi:10.20944/preprints202307.1065.v1

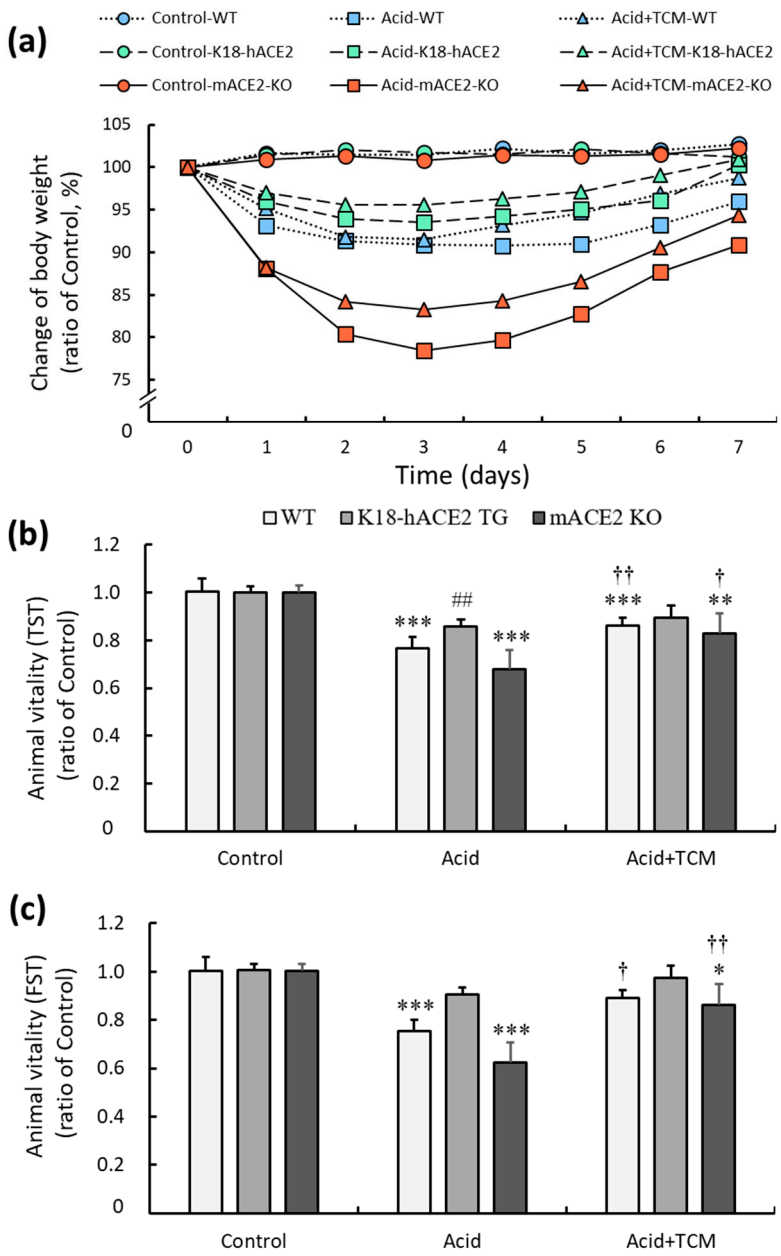

Figure 2. Physiological changes in acid-induced ALI mice administered NRICM101. (a) Changes in the body weights of the mice during the experiments. The average body weight on Day 0 in each group was calculated as 100%. (**b**) The changes in animal vitality, as detected by the TST, were determined and compared to the average TST result on Day 0 in each group, which was calculated as 100%. (**c**) The changes in animal vitality, as detected by FST, were determined and compared ton the average FST result on Day 0 in each group, which was calculated as 100%. All values are expressed as the mean ± SD for each group (n = 5); *$p < 0.05$, **$p < 0.01$ and ***$p < 0.001$ *vs*. Control group; †$p < 0.05$ and ††$p < 0.01$ *vs*. Acid group; ##$p < 0.01$ *vs*. WT mice. TST: tail suspension test; FST: forced swimming test. Control group: The mice were treated twice with phosphate buffered saline (PBS) intratracheal instillation. Acid group: The mice were treated twice with acid intratracheal instillation. Acid+TCM group: The mice were treated twice with acid intratracheal instillation and then administered NRICM101 for 4 days.

3.3. ACE2 and NRICM101 decreased lung permeability in ALI mice induced by acid instillation

Lung permeability is one of the indicators of lung injury. Evans blue dye (EBD) was used to investigate the permeability of blood vessels and cell membranes in the lungs. The results are shown

Preprints (www.preprints.org) | NOT PEER-REVIEWED | Posted: 17 July 2023 doi:10.20944/preprints202307.1065.v1

in **Figure 3**a. EBD was distributed throughout the lungs in the Acid group, whereas EBD in the Control group was only present near the trachea. In the Acid group, the EBD levels of WT, K18-hACE2 TG and mACE2 KO mice were significantly increased by 149, 112, and 178 μg/mL, respectively. In the Acid+TCM group, the EBD levels of WT, K18-hACE2 TG and mACE2 KO mice were reduced by approximately 130, 77 and 155 μg/mL, respectively (**Figure 3**b). Notably, in the Acid group, lung permeability was higher in mACE2 KO mice than in K18-hACE2 TG mice. After 4 days NRICM101 administration, lung permeability was reduced in mice of all genotypes compared with mice in the Acid group.

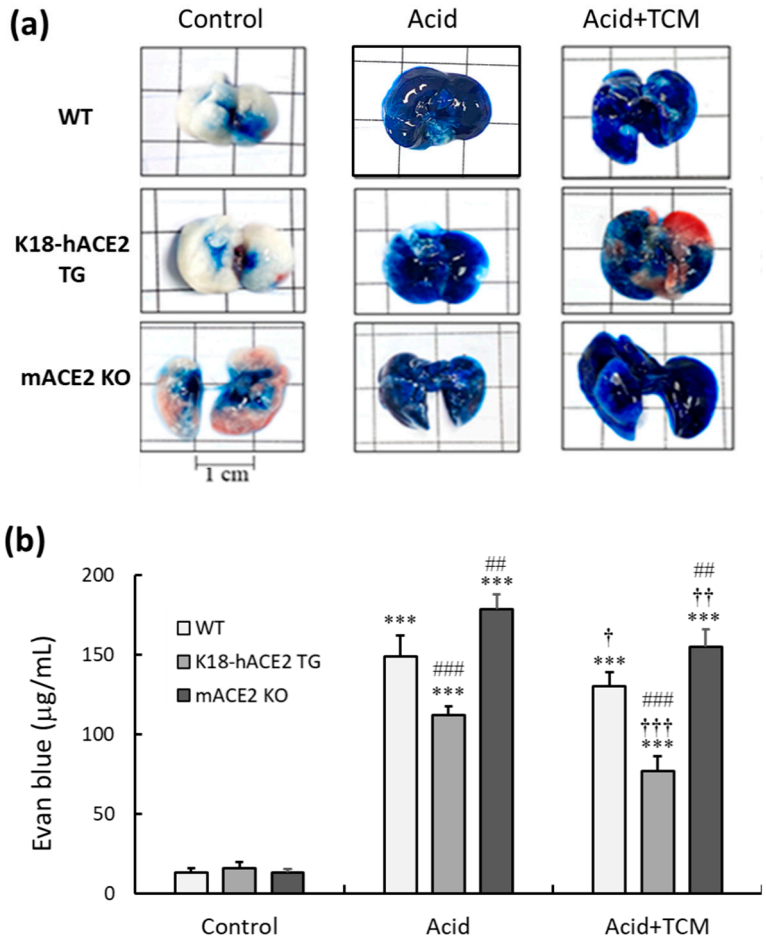

Figure 3. Changes in the lung permeability of mice with acid-induced ALI that were administered NRICM101. Before the experiment ended, EBD was intratracheally instillated into the lungs to observe lung permeability. (**a**) Representative images of Evans blue-stained lungs. (**b**) Histogram values reflect the mean ± SD (n = 5). The average value of Evans blue (μg/mL) in WT mice without acid intratracheal instillation or NRICM101 administration was calculated as 100%. Then, the related values of each group were calculated based on the value of the WT Control group. ***$p < 0.001$ *vs.* Control group; ††$p < 0.01$ and †††$p < 0.001$ *vs.* Acid group; ##$p < 0.01$ and ###$p < 0.001$ *vs.* WT mice.

3.4. ACE2 and NRICM101 reversed histopathological changes in ALI mice

Analysis of hematoxylin & eosin (H&E)-stained alveolar and bronchiolar sections from WT, K18-hACE2 TG, and mACE2 KO mice showed a progressive inflammatory process. In the Acid group, white blood cells (WBCs) infiltrated a greater area of the lung into adjacent alveolar spaces with airway epithelial thickening. In the Acid+TCM group, the extent of infiltration and airway epithelial thickening was decreased but was still more severe than that in the Control group (**Figure 4**). The lung tissue sections were also stained with Masson's trichrome to examine fibrotic pathology. In the

Preprints (www.preprints.org) | NOT PEER-REVIEWED | Posted: 17 July 2023 doi:10.20944/preprints202307.1065.v1

Acid group, massive collagen deposition was observed throughout the alveolar and bronchial walls of WT, K18-hACE2 TG, and mACE2 KO mice (**Figure 4**). In the Acid+TCM group, collagen deposition was decreased but was more severe than that in the Control group. Moreover, acid-induced ALI pathological changes in mACE2 KO mice were far greater than those in K18-hACE2 TG mice. The pathological features of ALI mice, including WBC infiltration, alveolar disruption and thickened airway epithelium by acid instillation, were slightly to moderately restored by NRICM101 administration.

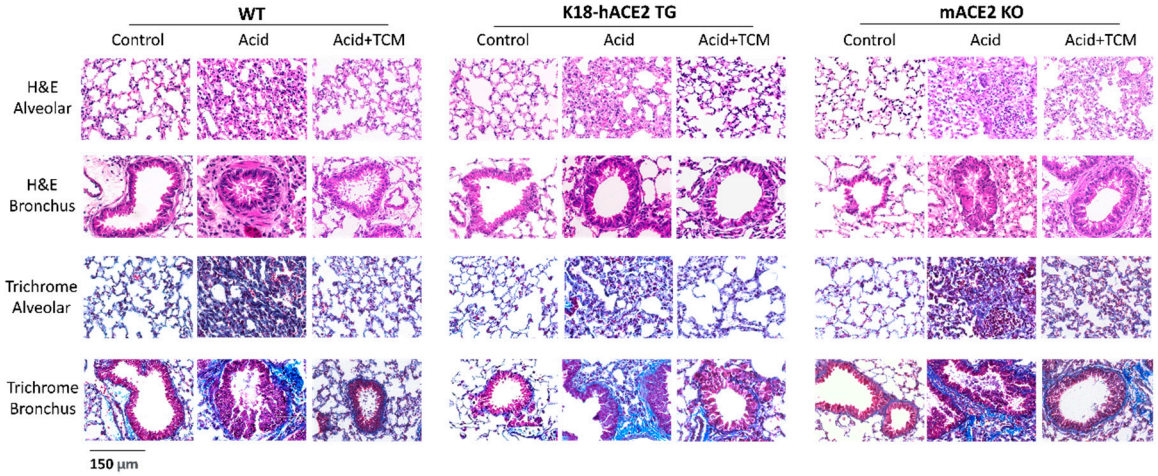

Figure 4. Bronchial and alveolar pathologic findings of acid-induced ALI mice and ALI mice administered NRICM101. Bronchial and alveolar sections of mouse lungs were stained with H&E to determine their pathological features. Leukocyte infiltration of the alveoli and significant thickening of the bronchial wall were observed in the lung sections of ALI mice. This pathological damage was significantly decreased in ALI mice administered NRICM101. The lung sections of mice were stained with trichrome blue to determine pathological changes. Alveolar fusion and collagen deposition, which indicate fibrosis, were observed in ALI mice. The fibrosis levels were significantly reduced in ALI mice administered NRICM101.

3.5. ACE2 and NRICM101 ameliorated pulmonary inflammation in ALI mice

In the Acid group, IL-6, TNF-α and TGF-β1 levels in the bronchoalveolar lavage fluid (BALF) were increased by 2.0-, 1.6- and 1.9-fold in WT mice, 1.1-, 1.1- and 1.2-fold in K18-hACE2 TG mice and 2.5-, 2.2- and 2.6-fold in mACE2 KO mice, respectively, compared with those in the Control group (**Figure 5**). In particular, IL-6 and TGF-β1 levels in mACE2 KO mice were significantly higher than those in the other mice with acid intratracheal instillation. In the Acid+TCM group, IL-6, TNF-α and TGF-β1 levels in BALF were reduced by approximately 1.3-, 1.4- and 1.5-fold in the WT mice; 1.0-, 1.0- and 1.1-fold in K18-hACE2 TG mice; and 1.8-, 1.5- and 1.9-fold in mACE2 KO mice, respectively, compared with those in the Control group (**Figure 5**). Interestingly, levels of inflammatory cytokines in K18-hACE2 TG mice with acid instillation and NRICM101 administration were similar to their basal levels.

Preprints (www.preprints.org) | NOT PEER-REVIEWED | Posted: 17 July 2023 doi:10.20944/preprints202307.1065.v1

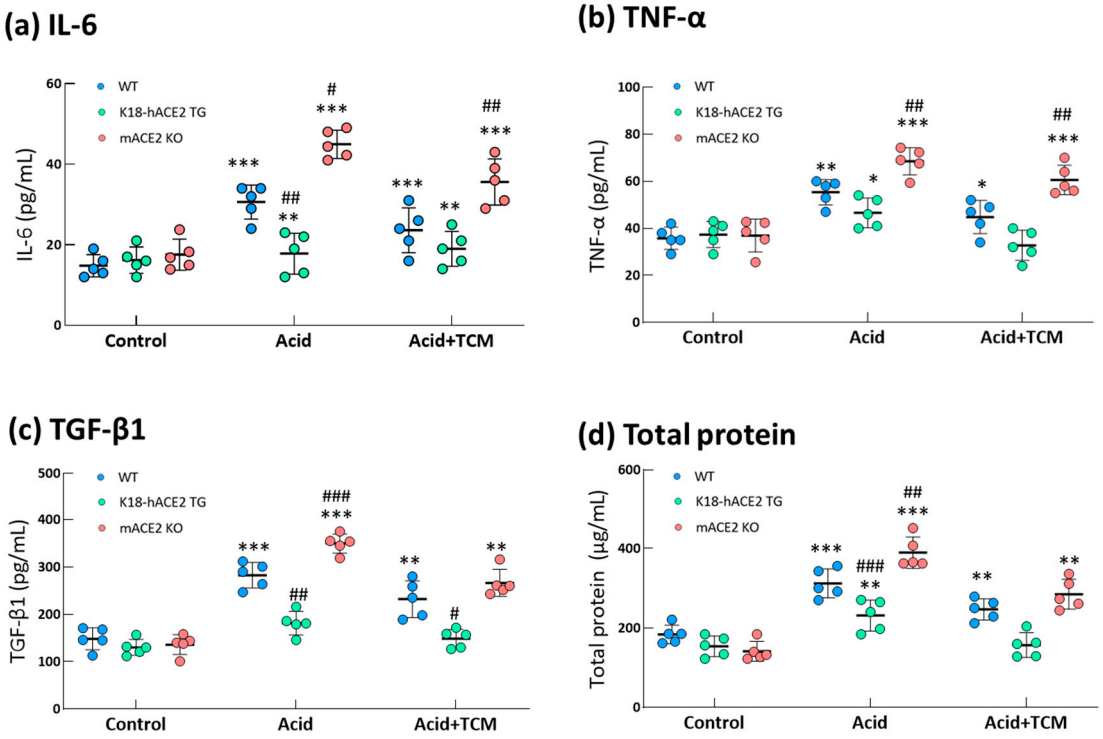

Figure 5. Changes in total protein and cytokines in the lungs of ALI mice administered NRICM101. Before the animals were sacrificed, BALF was collected from the mice to examine the IL-6, (**a**) TNF-α, and (**b**) TGF-β1 (**c**) and total protein (**d**) levels. The results showed that BALF total protein and cytokine levels in acid-treated mice were alleviated by NRICM101 administration. All values are expressed as the mean ± SD in each group (n = 5). *$p < 0.05$, **$p < 0.01$ and ***$p < 0.001$ *vs.* Control group; #$p < 0.05$, ##$p < 0.01$, ###$p < 0.001$ *vs.* WT mice.

3.6. NRICM101 administration countered the imbalance in ACE in ALI mice

To identify the RAS mediators associated with acid-induced ALI, the protein expression of ACE was investigated. In the Acid group, ACE expression in WT, K18-hACE2 TG, and mACE2 KO mice was increased by approximately 2.0-, 1.2- and 6-fold, respectively, compared with that in the Control group. There was no change in ACE expression in K18-hACE2 TG mice with acid intratracheal instillation. In the Acid+TCM group, ACE expression in WT, K18-hACE2 TG, and mACE2 KO mice was decreased 1.2-, 1.2- and 4.5-fold, respectively, compared with that in the Control group (**Figure 6**).

Preprints (www.preprints.org) | NOT PEER-REVIEWED | Posted: 17 July 2023 doi:10.20944/preprints202307.1065.v1

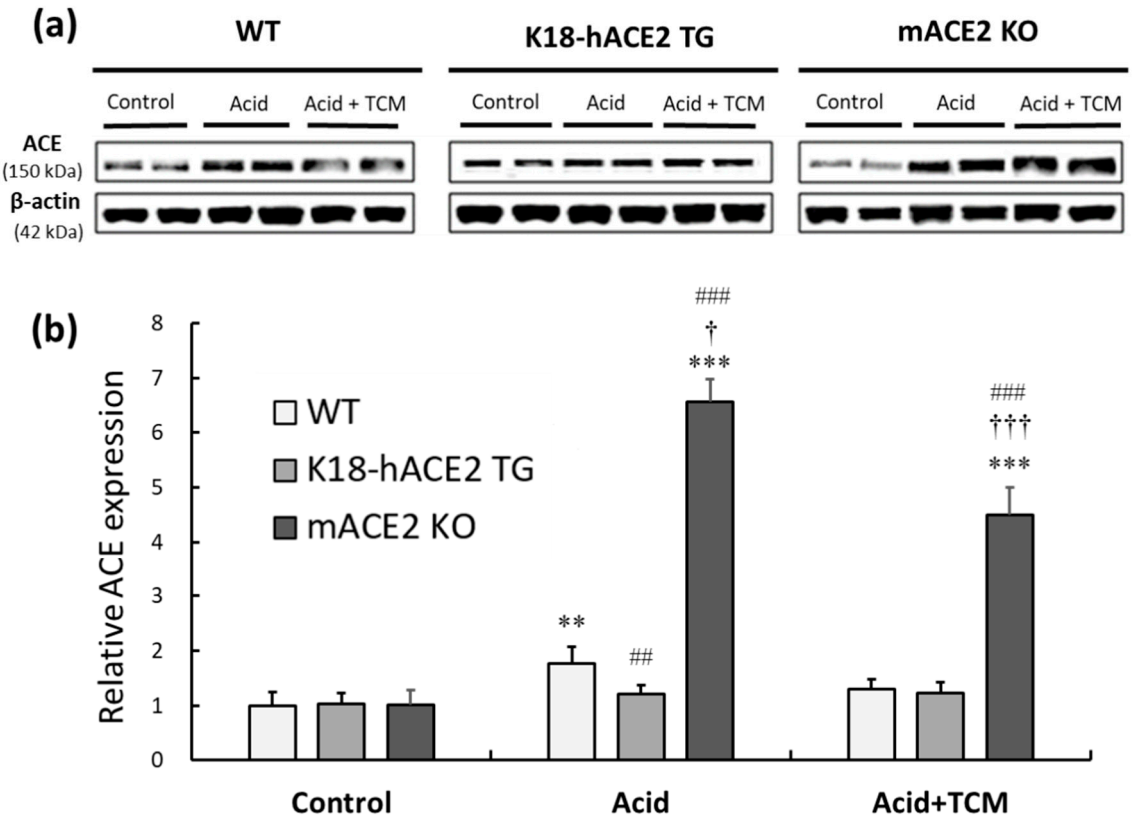

Figure 6. Relative ACE expression in the lungs of ALI mice administered NRICM101. (**a**) ACE expression (approximately 150 kDa) was validated by western blotting. (**b**) The relative ACE expression level (ACE/β-actin) was quantitated. Acid intratracheal instillation significantly induced pulmonary ACE expression, and the level of ACE was decreased in mice administered NRICM101. All values are expressed as the mean ± SD in each group (n = 5). $^{**}p < 0.01$ and $^{***}p < 0.001$ *vs*. Control group; †$p < 0.05$ and †††$p < 0.001$ *vs*. Acid group; ##$p < 0.01$ and ###$p < 0.001$ *vs*. WT mice.

3.7. ACE2 and NRICM101 alleviated STAT3 and ERK1/2 phosphorylation in the lungs of ALI mice

These results show that the levels of inflammatory cytokines were significantly induced after acid intratracheal instillation. IL-6, TNF-α and TGF-β1 participate in inflammatory responses by activating the STAT3 and ERK1/2 signaling pathways. Therefore, pERK1/2 and p STAT3 in lung tissues were detected by western blotting (**Figure 7**a).

The results showed that pulmonary phosphorylated-STAT3 (p-STAT3) levels in WT and mACE2 KO mice were significantly increased by 3.1- and 4.8-fold, respectively, after acid instillation, but there was no significant effect on K18-hACE2 TG mice (**Figure 7**b). Similarly, pulmonary phosphorylated-ERK1/2 (p-ERK1/2) levels in WT and mACE2 KO mice were significantly increased by 3.3- and 4.2-fold, respectively, after acid intratracheal instillation (**Figure 7**c). Conversely, WT and mACE2 KO mice in the Acid+TCM group had significantly downregulated expression of p-STAT3 and p-ERK1/2 compared to the Acid group (**Figure 7**).

Preprints (www.preprints.org) | NOT PEER-REVIEWED | Posted: 17 July 2023 doi:10.20944/preprints202307.1065.v1

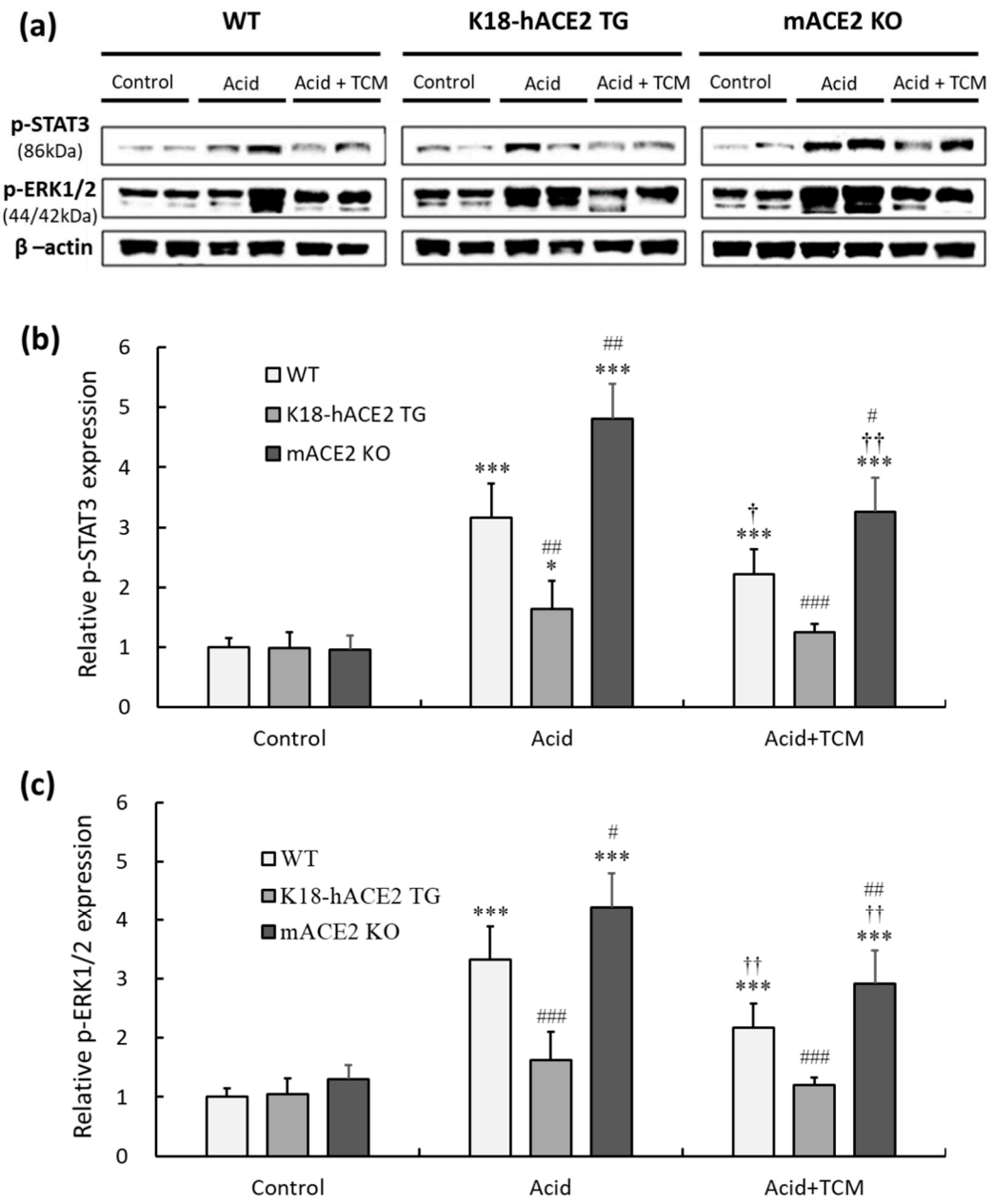

Figure 7. Relative p-STAT3 and p-ERK 1/2 expression in the lungs of ALI mice administered NRICM101. (**a**) p-STAT3 (150 kDa) and p-ERK1/2 (44/42 kDa) expression was validated by western blotting. (**b**) Relative quantitative analysis of p-STAT3. (**c**) Relative quantitative analysis of p-ERK1/2. Acid intratracheal instillation significantly induced pulmonary p-STAT3 and p-ERK 1/2 expression, and the increases in p-STAT3 and p-ERK 1/2 were ameliorated in the mice administered NRICM101. All values are expressed as the mean ± SD in each group (n = 5); *$p < 0.05$ and ***$p < 0.001$ *vs*. Control group; †$p < 0.05$ and ††$p < 0.01$ *vs*. Acid group; #$p < 0.05$, ##$p < 0.01$, ###$p < 0.001$ *vs*. WT mice.

3.8. ACE2 and NRICM101 modulated pulmonary gelatinase activity in mice with acid-induced ALI

Gelatinase containing MMP-2 and MMP-9 was measured by gelatin zymography (**Figure 8**a). In the Acid group, the MMP-2 activity of WT, K18-hACE2 TG and mACE2 KO mice was increased by approximately 1.9-, 1.1- and 2.7-fold, respectively, compared with that in the Control group (**Figure 8**b). Similarly, MMP-9 activity in WT, K18-hACE2 TG and mACE2 KO mice in the Acid group was increased by approximately 2.6-, 1.3- and 3.7-fold, respectively, compared to the Control group (**Figure 8**c). Gelatinase activity was significantly increased in the lungs of WT and mACE2 KO mice after acid instillation, but there was no significant change in the lungs of K18-hACE2 TG mice.

Preprints (www.preprints.org) | NOT PEER-REVIEWED | Posted: 17 July 2023 doi:10.20944/preprints202307.1065.v1

Furthermore, in the Acid+TCM group, the MMP-2 activity of WT, K18-hACE2 TG and mACE2 KO mice was reduced by 0.9-, 1.0- and 2.1-fold, respectively, compared to the Control group. However, MMP-9 activity was reduced 2.0-, 1.3- and 3.0-fold in WT, K18-hACE2 TG and mACE2 KO mice, respectively. The gelatinase activity of the WT and mACE2 KO mice in the Acid+TCM group was significantly changed compared to that in the Acid group.

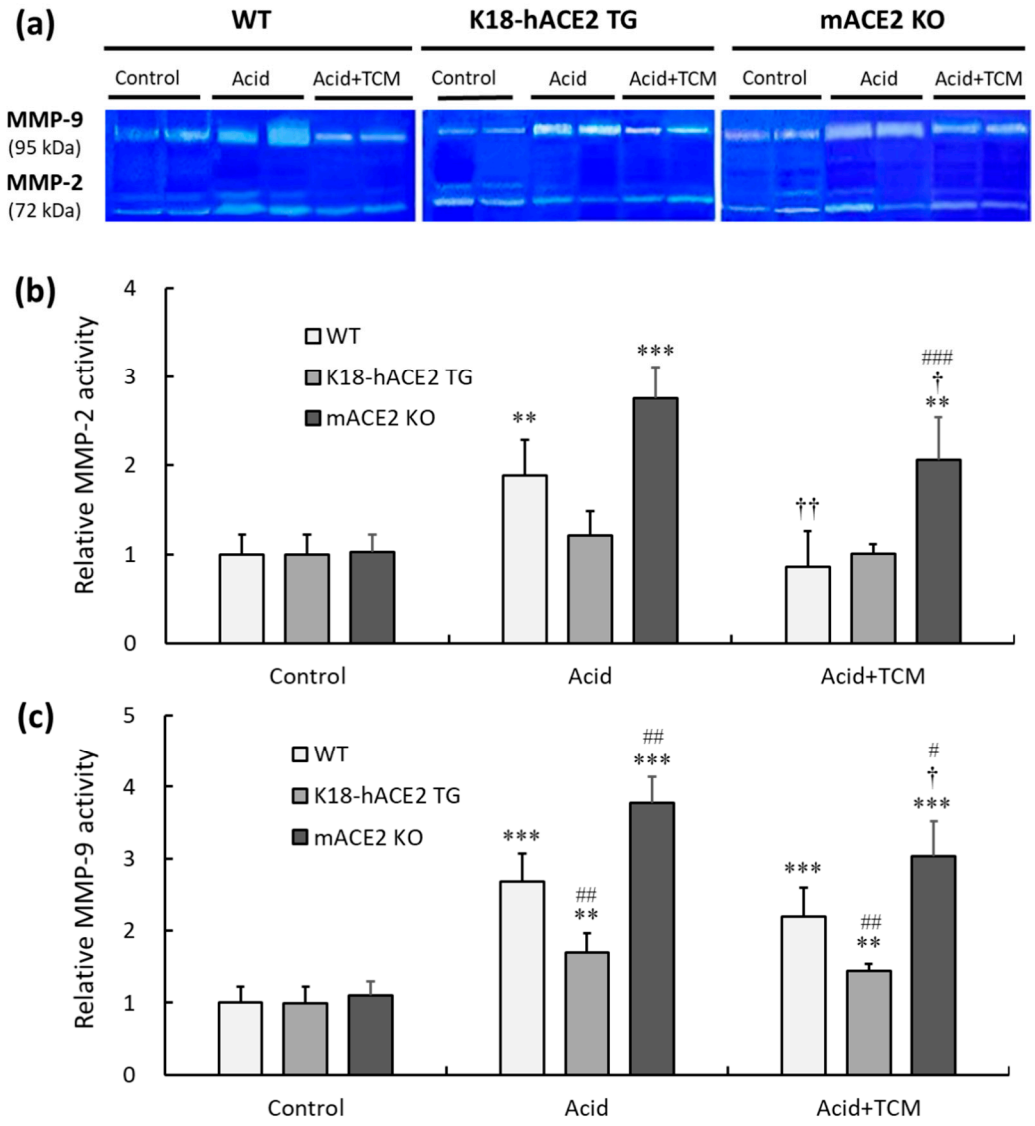

Figure 8. Relative MMP-2 and MMP-9 activity in the lungs of ALI mice administered NRICM101. (**a**) MMP-2 (72 kDa) and MMP-9 (95 kDa) activity in the lung was detected by gelatin zymography. (**b**) Relative quantitative analysis of MMP-2 activity. (**c**) Relative quantitative analysis of MMP-9 activity. Acid intratracheal instillation significantly induced pulmonary MMP-2 and MMP-9 activity, and the increase in MMP activity was alleviated in mice administered NRICM101. All values are expressed as the mean ± SD in each group (n = 5). $^{**}p < 0.01$ and $^{***}p < 0.001$ *vs*. Control group; †$p < 0.05$ and ††$p < 0.01$ *vs*. Acid group; #$p < 0.05$, ##$p < 0.01$, ###$p < 0.001$ *vs*. WT mice.

4. Discussion

Recently, the animal model of K18-hACE2 TG mice has been widely used in COVID-19 studies, including studies of vaccine evaluation and antiviral agents to combat SARS-CoV-2 [37,38]. The rapid inflammatory response and observed respiratory pathology after K18-hACE2 TG mice were challenged with SARS-CoV-2 resembles COVID-19 [38]. In fact, K18-hACE2 TG mice were originally

 doi:10.20944/preprints202307.1065.v1

and successfully developed for a SARS-CoV study in 2007 [39]. ACE2 has physiological roles as a SARS-CoV-2 entry receptor and in ALI or acute respiratory distress syndrome (ARDS) [40]. Although human ACE2 (hACE2), which is the entry receptor for SARS-CoV-2, has been well established, the contribution of the enzymatic functions of ACE2 to the pathogenesis of COVID-19-related lung injury has been a matter of debate [41]. Most likely, the double-edged sword of ACE2 related to SARS-CoV-2 pathogenicity can unravel these mysteries through investigations of mice with ACE2 genetic modifications [22–24].

In this study, acid intratracheal instillation in mice induced an inflammatory response and induced the production of the inflammatory cytokines IL-6, TNF-α, and TGF-β1 in the lungs. Several pulmonary diseases, such as ALI, ARDS, asthma, COPD and COVID-19 pneumonia, are associated with abnormal IL-6, TNF-α, and TGF-β1 expression [42–44]. Our results showed that IL-6, TNF-α, and TGF-β1 levels in the lungs of WT and mACE2 KO mice were significantly increased 4 days after acid instillation. Moreover, the lung sections of WT and ACE2 KO mice showed serious immunocyte infiltration and alveolar injury. These pathological features were also observed in the lungs of K18-hACE2 TG mice with mild symptoms. These data suggest that the overproduction of ACE2 and induction of the ACE2-Ang-(1-7)/Mas axis could reduce the inflammation induced by acid treatment. This finding was confirmed by many publications [45–47]. Activation of the ACE2-Ang-(1-7)/Mas receptor axis is absent in mACE2 KO mice, which exhibited severe injuries and imbalance in the RAS system compared with K18-hACE2 TG mice [48]. Additionally, an increase in ACE is associated with ALI. Based on these findings, robust increases in ACE protein expression were measured in acid-induced ALI. The upregulation of ACE and depletion of ACE2 could result in an imbalance in ACE/ACE2 [49–51], such as increasing the ACE/ACE2 ratio to accelerate the disease progression of acid-induced ALI or COVID-19 ALI.

ALI is characterized by the induction of inflammatory cytokines, such as IL-6, TNF-α and TGF-β1. These cytokines could participate in the MAPK, ERK1/2, and/or STAT3 pathways [52]. TGF-β1 mediates lung injury by increasing ROS levels [53] and activating extracellular matrix production, such as collagen and gelatin [54]. In addition, MMPs have been observed in a wide variety of pulmonary pathologies and could be regulated by MAPK signaling [55]. Members of the MMP family, especially the gelatinases MMP-2 and MMP-9, have been implicated in pulmonary inflammation and diseases, including asthma, ALI and pulmonary fibrosis [55,56]. Some studies have shown that MMP-2 and MMP-9 expression can be regulated by ACE2 [57,58]. We proposed that MMP regulation was responsible for the anti-inflammatory and/or antifibrotic effects on the lungs during acid-induced injury. MMP-2 is synthesized by structural cells, including fibroblasts and endothelial and epithelial cells; MMP-2 is associated with impaired tissue remodeling, thus leading to pathological collagen deposition and pulmonary fibrosis [59,60]. In contrast, MMP-9 is mainly secreted by neutrophils, eosinophils, mast cells, and alveolar macrophages and is associated with acute inflammation [61]. Studies have shown that SARS-CoV-2 infection can upregulate MMP-2 or MMP-9 expression in lung tissue [62]. Additionally, there is evidence to suggest that ACE2 deficiency can contribute to the dysregulation of gelatinase activity in COVID-19 [63,64]. Our data are consistent with the conclusions of previous studies. Our results showed that acid instillation activated MAPK signaling and then induced marked increases in pulmonary MMP-2 and MMP-9 in acid-treated mACE2 KO and WT mice but not in K18-hACE2 TG mice.

There have been numerous reports on the antiviral properties of dozens of Chinese herbs and hundreds of TCM ingredients [65]. TCM formulations have also been used to treat previous pandemics, including severe acute respiratory syndrome coronavirus (SARS-CoV) and Middle East respiratory syndrome coronavirus (MERS-CoV) outbreaks [66,67]. In recent years, TCM formulations have been developed to treat COVID-19 [68,69]. In Taiwan, the prescription used in general mild patients is Taiwan NRICM101, which was announced in May 2020, and the clinical results were reported in August 2022 [70]. In a mouse model, Taiwan NRICM101 exerted antiviral effects by reducing the affinity between the viral spike protein and ACE2 and suppressed IL-6 and TNF-α production in alveoli [34]. Thus, evidence can support the therapeutic effects of NRICM101 on COVID-19 treatment with at least two targeting mechanisms: preventing SARS-CoV-2 infection and

reducing the inflammation induced by the virus. According to Tsai et al. [34], NRICM101 has a multitarget mechanism of action. NRICM101 can block the binding of the ACE2 protein and spike protein to prevent virus infection and prevent viral replication by inhibiting the activity of viral 3CLpro [34]. Our data show that NRICM101 is effective against COVID-19, which corresponds to the more recent publications by Chang et al. [71] and Singh et al. [72].

5. Conclusions

The COVID-19 pandemic has caused continuing challenges to global health. It is still prudent to accelerate investigations of new therapeutic advances that can effectively treat COVID-19. Effective animal models for COVID-19 studies need to be developed because using SARS-CoV-2 greatly limits routine research. The most common and severe complication of COVID-19 is ALI, which can lead to respiratory failure and death. ACE2 is the receptor for SARS-CoV-2 entry into cells, and ACE2 plays a protective role in diseases of the respiratory system, such as ALI. It is important to validate the interaction between ACE2 and ALI, especially COVID-19-related ALI. The present study is the first report that used mice with *Ace2* gene modifications, including hACE2 transgenic mice and ACE2 knockout mice, to establish mouse models of acid-induced ALI and study the role of ACE2 in molecular pathogenesis. Our results indicated that ACE2 could counteract the proinflammatory effect of ALI and attenuate ALI pathogenesis. ACE2 effectively alleviates the pathogenic process of ALI by regulating MAPK, STAT3 and MMP activation. Finally, the TCM formula NRICM101, which has been used to prevent and treat COVID-19, shows potential for treating ALI.

6. Patents

Author Contributions: Conceptualization, C.-H.L. and C.-S.L.; writing-original draft preparation, C.-H.L., Y.-J.C. and M.-W.L.; writing-review and editing, C.-H.L., Y.-J.C.; M.-W.L. and C.-S.L.; Investigation, C.-H.L. Y.-J.C., H.-J.C., and X.-R.Y.; Supervision, C.-S.L. All authors have read and agreed to the published version of the manuscript.

Funding: This work received no external funding.

Institutional Review Board Statement: Not applicable.

Informed Consent Statement: All data in this study were obtained from published material in scientific journals, referenced in the paper, and can be obtained by any individual with access.

Data Availability Statement: The data presented in this study are available upon request from the corresponding author.

Acknowledgments: This work was supported by the grants of NSTC 110-2312-B-A49-001-MY3, NSTC 112-2811-B-A49-501 and NSTC 112-2321-B-A49-005, from the National Science and Technology Council (NSTC), Taiwan. This work was also financially supported by the "Center for Intelligent Drug Systems and Smart Bio-devices (IDS²B)" from The Featured Areas Research Center Program within the framework of the Higher Education Sprout Project of the National Yang Ming Chiao Tung University and Ministry of Education (MOE), Taiwan.

Conflicts of Interest: All of the authors declare no competing conflict of interest.

References

1. Fleming, I.; Kohlstedt, K.; Busse, R. The tissue renin-angiotensin system and intracellular signalling. *Curr Opin Nephrol Hypertens* **2006**, *15*, 8-13, doi:10.1097/01.mnh.0000196146.65330.ea.
2. Imai, Y.; Kuba, K.; Ohto-Nakanishi, T.; Penninger, J.M. Angiotensin-converting enzyme 2 (ACE2) in disease pathogenesis. *Circ J* **2010**, *74*, 405-410, doi:10.1253/circj.cj-10-0045.
3. Corvol, P.; Williams, T.A.; Soubrier, F. Peptidyl dipeptidase A: angiotensin I-converting enzyme. *Methods Enzymol* **1995**, *248*, 283-305, doi:10.1016/0076-6879(95)48020-x.
4. Vickers, C.; Hales, P.; Kaushik, V.; Dick, L.; Gavin, J.; Tang, J.; Godbout, K.; Parsons, T.; Baronas, E.; Hsieh, F.; et al. Hydrolysis of biological peptides by human angiotensin-converting enzyme-related carboxypeptidase. *J Biol Chem* **2002**, *277*, 14838-14843, doi:10.1074/jbc.M200581200.

5. Donoghue, M.; Hsieh, F.; Baronas, E.; Godbout, K.; Gosselin, M.; Stagliano, N.; Donovan, M.; Woolf, B.; Robison, K.; Jeyaseelan, R.; et al. A novel angiotensin-converting enzyme-related carboxypeptidase (ACE2) converts angiotensin I to angiotensin 1-9. *Circ Res* **2000**, *87*, E1-9, doi:10.1161/01.res.87.5.e1.
6. Tipnis, S.R.; Hooper, N.M.; Hyde, R.; Karran, E.; Christie, G.; Turner, A.J. A human homolog of angiotensin-converting enzyme: cloning and functional expression as a captopril-insensitive carboxypeptidase. *Journal of Biological Chemistry* **2000**, *275*, 33238-33243.
7. Mizuiri, S.; Ohashi, Y. ACE and ACE2 in kidney disease. *World J Nephrol* **2015**, *4*, 74-82, doi:10.5527/wjn.v4.i1.74.
8. Soler, M.J.; Batlle, M.; Riera, M.; Campos, B.; Ortiz-Perez, J.T.; Anguiano, L.; Roca-Ho, H.; Farrero, M.; Mont, L.; Pascual, J.; et al. ACE2 and ACE in acute and chronic rejection after human heart transplantation. *Int J Cardiol* **2019**, *275*, 59-64, doi:10.1016/j.ijcard.2018.10.002.
9. Zamai, L. The Yin and Yang of ACE/ACE2 Pathways: The Rationale for the Use of Renin-Angiotensin System Inhibitors in COVID-19 Patients. *Cells* **2020**, *9*, doi:10.3390/cells9071704.
10. Santos, R.A.; e Silva, A.C.S.; Maric, C.; Silva, D.M.; Machado, R.P.; de Buhr, I.; Heringer-Walther, S.; Pinheiro, S.V.B.; Lopes, M.T.; Bader, M. Angiotensin-(1–7) is an endogenous ligand for the G protein-coupled receptor Mas. *Proceedings of the National Academy of Sciences* **2003**, *100*, 8258-8263.
11. Mercure, C.; Yogi, A.; Callera, G.E.; Aranha, A.B.; Bader, M.; Ferreira, A.J.; Santos, R.A.; Walther, T.; Touyz, R.M.; Reudelhuber, T.L. Angiotensin(1-7) blunts hypertensive cardiac remodeling by a direct effect on the heart. *Circ Res* **2008**, *103*, 1319-1326, doi:10.1161/CIRCRESAHA.108.184911.
12. Zhou, P.; Yang, X.L.; Wang, X.G.; Hu, B.; Zhang, L.; Zhang, W.; Si, H.R.; Zhu, Y.; Li, B.; Huang, C.L.; et al. A pneumonia outbreak associated with a new coronavirus of probable bat origin. *Nature* **2020**, *579*, 270-273, doi:10.1038/s41586-020-2012-7.
13. Available online: https://coronavirus.jhu.edu/map.html (accessed on
14. Wilhelm, E.; Ballalai, I.; Belanger, M.-E.; Benjamin, P.; Bertrand-Ferrandis, C.; Bezbaruah, S.; Briand, S.; Brooks, I.; Bruns, R.; Bucci, L.M. Measuring the burden of infodemics: Summary of the methods and results of the Fifth WHO Infodemic Management Conference. *JMIR infodemiology* **2023**, *3*, e44207.
15. Ni, W.; Yang, X.; Yang, D.; Bao, J.; Li, R.; Xiao, Y.; Hou, C.; Wang, H.; Liu, J.; Yang, D.; et al. Role of angiotensin-converting enzyme 2 (ACE2) in COVID-19. *Crit Care* **2020**, *24*, 422, doi:10.1186/s13054-020-03120-0.
16. Banu, N.; Panikar, S.S.; Leal, L.R.; Leal, A.R. Protective role of ACE2 and its downregulation in SARS-CoV-2 infection leading to Macrophage Activation Syndrome: Therapeutic implications. *Life Sci* **2020**, *256*, 117905, doi:10.1016/j.lfs.2020.117905.
17. South, A.M.; Diz, D.I.; Chappell, M.C. COVID-19, ACE2, and the cardiovascular consequences. *Am J Physiol Heart Circ Physiol* **2020**, *318*, H1084-H1090, doi:10.1152/ajpheart.00217.2020.
18. Garcia, G.E.; Truong, L.D.; Johnson, R.J. Angiotensin-converting enzyme 2 decreased expression during kidney inflammatory diseases: implications to predisposing to COVID-19 kidney complications. *Kidney Int* **2021**, *100*, 1138-1140, doi:10.1016/j.kint.2021.08.016.
19. Yan, R.; Zhang, Y.; Li, Y.; Xia, L.; Guo, Y.; Zhou, Q. Structural basis for the recognition of SARS-CoV-2 by full-length human ACE2. *Science* **2020**, *367*, 1444-1448, doi:10.1126/science.abb2762.
20. Rockx, B.; Baas, T.; Zornetzer, G.A.; Haagmans, B.; Sheahan, T.; Frieman, M.; Dyer, M.D.; Teal, T.H.; Proll, S.; van den Brand, J.; et al. Early upregulation of acute respiratory distress syndrome-associated cytokines promotes lethal disease in an aged-mouse model of severe acute respiratory syndrome coronavirus infection. *J Virol* **2009**, *83*, 7062-7074, doi:10.1128/JVI.00127-09.
21. Klein, N.; Gembardt, F.; Supe, S.; Kaestle, S.M.; Nickles, H.; Erfinanda, L.; Lei, X.; Yin, J.; Wang, L.; Mertens, M.; et al. Angiotensin-(1-7) protects from experimental acute lung injury. *Crit Care Med* **2013**, *41*, e334-343, doi:10.1097/CCM.0b013e31828a6688.
22. South, A.M.; Tomlinson, L.; Edmonston, D.; Hiremath, S.; Sparks, M.A. Controversies of renin-angiotensin system inhibition during the COVID-19 pandemic. *Nat Rev Nephrol* **2020**, *16*, 305-307, doi:10.1038/s41581-020-0279-4.
23. Wang, K.; Gheblawi, M.; Oudit, G.Y. Angiotensin Converting Enzyme 2: A Double-Edged Sword. *Circulation* **2020**, *142*, 426-428, doi:10.1161/CIRCULATIONAHA.120.047049.
24. Yan, T.; Xiao, R.; Lin, G. Angiotensin-converting enzyme 2 in severe acute respiratory syndrome coronavirus and SARS-CoV-2: A double-edged sword? *FASEB J* **2020**, *34*, 6017-6026, doi:10.1096/fj.202000782.
25. Control, C.f.D.; Prevention. Interim laboratory biosafety guidelines for handling and processing specimens associated with coronavirus disease 2019 (COVID-19). **2021**.
26. Muñoz-Fontela, C.; Dowling, W.E.; Funnell, S.G.; Gsell, P.-S.; Riveros-Balta, A.X.; Albrecht, R.A.; Andersen, H.; Baric, R.S.; Carroll, M.W.; Cavaleri, M. Animal models for COVID-19. *Nature* **2020**, *586*, 509-515.
27. Johansen, M.; Irving, A.; Montagutelli, X.; Tate, M.; Rudloff, I.; Nold, M.; Hansbro, N.; Kim, R.; Donovan, C.; Liu, G. Animal and translational models of SARS-CoV-2 infection and COVID-19. *Mucosal immunology* **2020**, *13*, 877-891.

28. Swenson, K.E.; Swenson, E.R. Pathophysiology of Acute Respiratory Distress Syndrome and COVID-19 Lung Injury. *Crit Care Clin* **2021**, *37*, 749-776, doi:10.1016/j.ccc.2021.05.003.
29. Hu, B.; Huang, S.; Yin, L. The cytokine storm and COVID-19. *J Med Virol* **2021**, *93*, 250-256, doi:10.1002/jmv.26232.
30. Yang, Y.; Islam, M.S.; Wang, J.; Li, Y.; Chen, X. Traditional Chinese Medicine in the Treatment of Patients Infected with 2019-New Coronavirus (SARS-CoV-2): A Review and Perspective. *Int J Biol Sci* **2020**, *16*, 1708-1717, doi:10.7150/ijbs.45538.
31. Ge, R. Targeting airway macrophages for inflammatory lung diseases-insights from traditional Chinese medicine. *Ann Transl Med* **2022**, *10*, 1086, doi:10.21037/atm-22-4845.
32. Zhao, J.; Yang, Y.; Huang, H.; Li, D.; Gu, D.; Lu, X.; Zhang, Z.; Liu, L.; Liu, T.; Liu, Y. Relationship between the ABO blood group and the coronavirus disease 2019 (COVID-19) susceptibility. *Clinical Infectious Diseases* **2021**, *73*, 328-331.
33. Ji, Z.; Hu, H.; Qiang, X.; Lin, S.; Pang, B.; Cao, L.; Zhang, L.; Liu, S.; Chen, Z.; Zheng, W.; et al. Traditional Chinese Medicine for COVID-19: A Network Meta-Analysis and Systematic Review. *Am J Chin Med* **2022**, *50*, 883-925, doi:10.1142/S0192415X22500379.
34. Tsai, K.-C.; Huang, Y.-C.; Liaw, C.-C.; Tsai, C.-I.; Chiou, C.-T.; Lin, C.-J.; Wei, W.-C.; Lin, S.J.-S.; Tseng, Y.-H.; Yeh, K.-M. A traditional Chinese medicine formula NRICM101 to target COVID-19 through multiple pathways: A bedside-to-bench study. *Biomedicine & Pharmacotherapy* **2021**, *133*, 111037.
35. Basoalto, R.; Damiani, L.F.; Bachmann, M.C.; Fonseca, M.; Barros, M.; Soto, D.; Araos, J.; Jalil, Y.; Dubo, S.; Retamal, J.; et al. Acute lung injury secondary to hydrochloric acid instillation induces small airway hyperresponsiveness. *Am J Transl Res* **2021**, *13*, 12734-12741.
36. Tavares, A.H.; Colby, J.K.; Levy, B.D.; Abdulnour, R.E. A Model of Self-limited Acute Lung Injury by Unilateral Intra-bronchial Acid Instillation. *J Vis Exp* **2019**, doi:10.3791/60024.
37. Zheng, J.; Wong, L.R.; Li, K.; Verma, A.K.; Ortiz, M.E.; Wohlford-Lenane, C.; Leidinger, M.R.; Knudson, C.M.; Meyerholz, D.K.; McCray, P.B., Jr.; et al. COVID-19 treatments and pathogenesis including anosmia in K18-hACE2 mice. *Nature* **2021**, *589*, 603-607, doi:10.1038/s41586-020-2943-z.
38. Yinda, C.K.; Port, J.R.; Bushmaker, T.; Offei Owusu, I.; Purushotham, J.N.; Avanzato, V.A.; Fischer, R.J.; Schulz, J.E.; Holbrook, M.G.; Hebner, M.J. K18-hACE2 mice develop respiratory disease resembling severe COVID-19. *PLoS pathogens* **2021**, *17*, e1009195.
39. McCray, P.B., Jr.; Pewe, L.; Wohlford-Lenane, C.; Hickey, M.; Manzel, L.; Shi, L.; Netland, J.; Jia, H.P.; Halabi, C.; Sigmund, C.D.; et al. Lethal infection of K18-hACE2 mice infected with severe acute respiratory syndrome coronavirus. *J Virol* **2007**, *81*, 813-821, doi:10.1128/JVI.02012-06.
40. Lin, H.; Liu, Q.; Zhao, L.; Liu, Z.; Cui, H.; Li, P.; Fan, H.; Guo, L. Circulating Pulmonary-Originated Epithelial Biomarkers for Acute Respiratory Distress Syndrome: A Systematic Review and Meta-Analysis. *Int J Mol Sci* **2023**, *24*, doi:10.3390/ijms24076090.
41. Oz, M.; Lorke, D.E. Multifunctional angiotensin converting enzyme 2, the SARS-CoV-2 entry receptor, and critical appraisal of its role in acute lung injury. *Biomedicine & Pharmacotherapy* **2021**, *136*, 111193.
42. Wei, J.; Xiong, X.-f.; Lin, Y.-h.; Zheng, B.-x.; Cheng, D.-y. Association between serum interleukin-6 concentrations and chronic obstructive pulmonary disease: a systematic review and meta-analysis. *PeerJ* **2015**, *3*, e1199.
43. Rincon, M.; Irvin, C.G. Role of IL-6 in asthma and other inflammatory pulmonary diseases. *Int J Biol Sci* **2012**, *8*, 1281-1290, doi:10.7150/ijbs.4874.
44. Rabaan, A.A.; Al-Ahmed, S.H.; Muhammad, J.; Khan, A.; Sule, A.A.; Tirupathi, R.; Mutair, A.A.; Alhumaid, S.; Al-Omari, A.; Dhawan, M.; et al. Role of Inflammatory Cytokines in COVID-19 Patients: A Review on Molecular Mechanisms, Immune Functions, Immunopathology and Immunomodulatory Drugs to Counter Cytokine Storm. *Vaccines (Basel)* **2021**, *9*, doi:10.3390/vaccines9050436.
45. Simoes e Silva, A.C.; Silveira, K.D.; Ferreira, A.J.; Teixeira, M.M. ACE2, angiotensin-(1-7) and Mas receptor axis in inflammation and fibrosis. *Br J Pharmacol* **2013**, *169*, 477-492, doi:10.1111/bph.12159.
46. Gaddam, R.R.; Chambers, S.; Bhatia, M. ACE and ACE2 in inflammation: a tale of two enzymes. *Inflamm Allergy Drug Targets* **2014**, *13*, 224-234, doi:10.2174/1871528113666140713164506.
47. Cantero-Navarro, E.; Fernandez-Fernandez, B.; Ramos, A.M.; Rayego-Mateos, S.; Rodrigues-Diez, R.R.; Sanchez-Nino, M.D.; Sanz, A.B.; Ruiz-Ortega, M.; Ortiz, A. Renin-angiotensin system and inflammation update. *Mol Cell Endocrinol* **2021**, *529*, 111254, doi:10.1016/j.mce.2021.111254.
48. Imai, Y.; Kuba, K.; Rao, S.; Huan, Y.; Guo, F.; Guan, B.; Yang, P.; Sarao, R.; Wada, T.; Leong-Poi, H.; et al. Angiotensin-converting enzyme 2 protects from severe acute lung failure. *Nature* **2005**, *436*, 112-116, doi:10.1038/nature03712.
49. Beyerstedt, S.; Casaro, E.B.; Rangel, E.B. COVID-19: angiotensin-converting enzyme 2 (ACE2) expression and tissue susceptibility to SARS-CoV-2 infection. *Eur J Clin Microbiol Infect Dis* **2021**, *40*, 905-919, doi:10.1007/s10096-020-04138-6.

50. Yang, C.W.; Lu, L.C.; Chang, C.C.; Cho, C.C.; Hsieh, W.Y.; Tsai, C.H.; Lin, Y.C.; Lin, C.S. Imbalanced plasma ACE and ACE2 level in the uremic patients with cardiovascular diseases and its change during a single hemodialysis session. *Ren Fail* **2017**, *39*, 719-728, doi:10.1080/0886022X.2017.1398665.
51. Lin, C.I.; Tsai, C.H.; Sun, Y.L.; Hsieh, W.Y.; Lin, Y.C.; Chen, C.Y.; Lin, C.S. Instillation of particulate matter 2.5 induced acute lung injury and attenuated the injury recovery in ACE2 knockout mice. *Int J Biol Sci* **2018**, *14*, 253-265, doi:10.7150/ijbs.23489.
52. Goodman, R.B.; Pugin, J.; Lee, J.S.; Matthay, M.A. Cytokine-mediated inflammation in acute lung injury. *Cytokine Growth Factor Rev* **2003**, *14*, 523-535, doi:10.1016/s1359-6101(03)00059-5.
53. Liu, R.M.; Desai, L.P. Reciprocal regulation of TGF-beta and reactive oxygen species: A perverse cycle for fibrosis. *Redox Biol* **2015**, *6*, 565-577, doi:10.1016/j.redox.2015.09.009.
54. Aschner, Y.; Downey, G.P. Transforming Growth Factor-beta: Master Regulator of the Respiratory System in Health and Disease. *Am J Respir Cell Mol Biol* **2016**, *54*, 647-655, doi:10.1165/rcmb.2015-0391TR.
55. Davey, A.; McAuley, D.F.; O'Kane, C.M. Matrix metalloproteinases in acute lung injury: mediators of injury and drivers of repair. *Eur Respir J* **2011**, *38*, 959-970, doi:10.1183/09031936.00032111.
56. Vandenbroucke, R.E.; Dejonckheere, E.; Libert, C. A therapeutic role for matrix metalloproteinase inhibitors in lung diseases? *Eur Respir J* **2011**, *38*, 1200-1214, doi:10.1183/09031936.00027411.
57. Shenoy, V.; Qi, Y.; Katovich, M.J.; Raizada, M.K. ACE2, a promising therapeutic target for pulmonary hypertension. *Curr Opin Pharmacol* **2011**, *11*, 150-155, doi:10.1016/j.coph.2010.12.002.
58. Kuan, T.C.; Chen, M.Y.; Liao, Y.C.; Ko, L.; Hong, Y.H.; Yen, C.Y.; Hsieh, W.Y.; Cheng, K.S.; Wu, C.L.; Lin, C.S. Angiotensin II downregulates ACE2-mediated enhancement of MMP-2 activity in human cardiofibroblasts. *Biochem Cell Biol* **2013**, *91*, 435-442, doi:10.1139/bcb-2013-0031.
59. Iwazu, Y.; Muto, S.; Hirahara, I.; Fujisawa, G.; Takeda, S.-i.; Kusano, E. Matrix metalloproteinase 2 induces epithelial-mesenchymal transition in proximal tubules from the luminal side and progresses fibrosis in mineralocorticoid/salt-induced hypertensive rats. *Journal of hypertension* **2011**, *29*, 2440-2453.
60. Eldred, J.A.; Hodgkinson, L.M.; Dawes, L.J.; Reddan, J.R.; Edwards, D.R.; Wormstone, I.M. MMP2 activity is critical for TGFβ2-induced matrix contraction—Implications for fibrosis. *Investigative ophthalmology & visual science* **2012**, *53*, 4085-4098.
61. Yoon, H.K.; Cho, H.Y.; Kleeberger, S.R. Protective role of matrix metalloproteinase-9 in ozone-induced airway inflammation. *Environ Health Perspect* **2007**, *115*, 1557-1563, doi:10.1289/ehp.10289.
62. C, D.A.-M.; Couto, A.E.S.; Campos, L.C.B.; Vasconcelos, T.F.; Michelon-Barbosa, J.; Corsi, C.A.C.; Mestriner, F.; Petroski-Moraes, B.C.; Garbellini-Diab, M.J.; Couto, D.M.S.; et al. MMP-2 and MMP-9 levels in plasma are altered and associated with mortality in COVID-19 patients. *Biomed Pharmacother* **2021**, *142*, 112067, doi:10.1016/j.biopha.2021.112067.
63. Kassiri, Z.; Zhong, J.; Guo, D.; Basu, R.; Wang, X.; Liu, P.P.; Scholey, J.W.; Penninger, J.M.; Oudit, G.Y. Loss of angiotensin-converting enzyme 2 accelerates maladaptive left ventricular remodeling in response to myocardial infarction. *Circ Heart Fail* **2009**, *2*, 446-455, doi:10.1161/CIRCHEARTFAILURE.108.840124.
64. Zhang, Z.; Chen, L.; Zhong, J.; Gao, P.; Oudit, G.Y. ACE2/Ang-(1-7) signaling and vascular remodeling. *Sci China Life Sci* **2014**, *57*, 802-808, doi:10.1007/s11427-014-4693-3.
65. Xian, Y.; Zhang, J.; Bian, Z.; Zhou, H.; Zhang, Z.; Lin, Z.; Xu, H. Bioactive natural compounds against human coronaviruses: a review and perspective. *Acta Pharm Sin B* **2020**, *10*, 1163-1174, doi:10.1016/j.apsb.2020.06.002.
66. Zhang, M.M.; Liu, X.M.; He, L. Effect of integrated traditional Chinese and Western medicine on SARS: a review of clinical evidence. *World J Gastroenterol* **2004**, *10*, 3500-3505, doi:10.3748/wjg.v10.i23.3500.
67. McKimm-Breschkin, J.L.; Jiang, S.; Hui, D.S.; Beigel, J.H.; Govorkova, E.A.; Lee, N. Prevention and treatment of respiratory viral infections: presentations on antivirals, traditional therapies and host-directed interventions at the 5th ISIRV Antiviral Group conference. *Antiviral research* **2018**, *149*, 118-142.
68. Huang, Y.F.; Bai, C.; He, F.; Xie, Y.; Zhou, H. Review on the potential action mechanisms of Chinese medicines in treating Coronavirus Disease 2019 (COVID-19). *Pharmacol Res* **2020**, *158*, 104939, doi:10.1016/j.phrs.2020.104939.
69. Xia, S.; Zhang, Y.; Wang, Y.; Wang, H.; Yang, Y.; Gao, G.F.; Tan, W.; Wu, G.; Xu, M.; Lou, Z. Safety and immunogenicity of an inactivated COVID-19 vaccine, BBIBP-CorV, in people younger than 18 years: a randomised, double-blind, controlled, phase 1/2 trial. *The Lancet Infectious Diseases* **2022**, *22*, 196-208.
70. Tseng, Y.-H.; Lin, S.J.-S.; Hou, S.-M.; Wang, C.-H.; Cheng, S.-P.; Tseng, K.-Y.; Lee, M.-Y.; Lee, S.-M.; Huang, Y.-C.; Lin, C.-J. Curbing COVID-19 progression and mortality with traditional Chinese medicine among hospitalized patients with COVID-19: A propensity score-matched analysis. *Pharmacological research* **2022**, *184*, 106412.
71. Cheng, Y.-D.; Lu, C.-C.; Hsu, Y.-M.; Tsai, F.-J.; Bau, D.-T.; Tsai, S.-C.; Cheng, C.-C.; Lin, J.-J.; Huang, Y.-Y.; Juan, Y.-N. In silico and in vitro studies of Taiwan Chingguan Yihau (NRICM101) on TNF-α/IL-1β-induced Human Lung Cells. *BioMedicine* **2022**, *12*, 56.
72. Singh, S.; Yang, Y.-F. Pharmacological Mechanism of NRICM101 for COVID-19 Treatments by Combined Network Pharmacology and Pharmacodynamics. *International Journal of Molecular Sciences* **2022**, *23*, 15385.

 doi:10.20944/preprints202307.1065.v1